Time migrated CRS images of complex inverted basin structures

E. Menyoli, D. Gajewski, and Ch. Hübscher

email: *menyoli@dkrz.de*
keywords: *CRS, time migration, thrustbelt*

ABSTRACT

In this paper we present poststack time migrated images of the Donbas Foldbelt (Ukraine) data. The unmigrated stacked section was generated after applying the common reflection surface (CRS) stack method. For this data, interpretation of the poststack time migrated section after conventional common midpoint stacking was difficult in certain areas of the line. The main fault zone which emerges at the surface is not clearly delineated in the conventionally migrated stacked section. We show that the CRS method when correctly applied gives enhanced stacked images in these areas. The subsequent poststack time migration of the CRS images reveals additional reflectors and improved reflector continuity. More steep dip events as well as deeper reflectors are recognized. This gives more information about the continuity of the fault system and enhances the interpretation in the identified zones of the profile.

INTRODUCTION

Seismic imaging in complex areas such as thrust belts and complex tectonics is hampered by several factors that often lead to poor quality data. Usually thrust faulting and folding produces locally very steep dips and strong lateral velocity variations, therefore violating the assumption of common reflection point traces which is used in conventional common midpoint stacking. Because of this violation, stacking velocity analysis and the subsequent stacking led to poorly unmigrated images. The data quality and the geology of the Donbas Foldbelt led to difficulties in seismic interpretation after applying conventional processing steps.

In some areas the interpretation of the poststack time migrated section was difficult. The imaging potential of the poststack migration was limited by the quality of the stacked section. Reflectors suddenly disappeared and in some areas their continuity was disrupted and it was difficult to interpret fault systems up-to the subsurface. Likewise in the deeper areas low signal to noise ratio resulted in poor images. The interpretation of the time section was essential for constructing layer boundaries and interval velocities. In order to improve the image quality of the identified areas, we used the zero offset CRS stack method (Mann et al., 1999) and later applied Kirchhoff poststack time migration. The improved quality and reflector continuity of the CRS stacked section is caused by the increased fold achieved by application of the CRS stacking operator.

The CRS stack uses a general stacking operator that describes the reflection moveout response for inhomogeneous media and no velocity analysis is required. Mann et al. (1999) demonstrated the strength of the CRS method on synthetic examples and real data as compared to the results from conventional CMP stacking after dip-moveout correction. The paper by Mann et al. (1999) gives a technical description of the CRS stack method. Here, we present results of applying CRS method and poststack time migration on the Donbas Foldbelt data which was acquired in 2000 in the framework of the DOBREflection 2000 project (Donbas Reflection 2000 Project).

GEOLOGIC SETTING AND PROCESSING

The Donbas Foldbelt (DF) is the eastern part of the Late Devonian Dniepr-Donets rift basin, located in southeastern Ukraine, lying between the Ukrainian Shield and the Voronezh Massif in Ukraine and Belarus (Figure 1). The basin is a Devonian rift basin with sediment thickness (comprising Late Devonian syn-rift and Carboniferous-Palaogene post-rift successions) increasing from about 2 km in the northeast to about 22 km in the deepest segment of the basin (Stovba and Stephenson, 1999). The Dniepr-Donets basin developed and evolved as a result of rifting and lithospheric extension. Rapid syn-rift subsidence occurred during lithospheric extension as the result of crystal thinning induced by lithospheric geothermic increase. In Early Permian times the DF was highly uplifted compared to the central and northeastern part of the basin. Folding, thrusting and reverse faulting mainly occurred in Late Cretaceous times. To elucidate the evolution of processes that occurred during rifting and rift reactivation, basin uplift and inversion, a seismic profile was acquired.

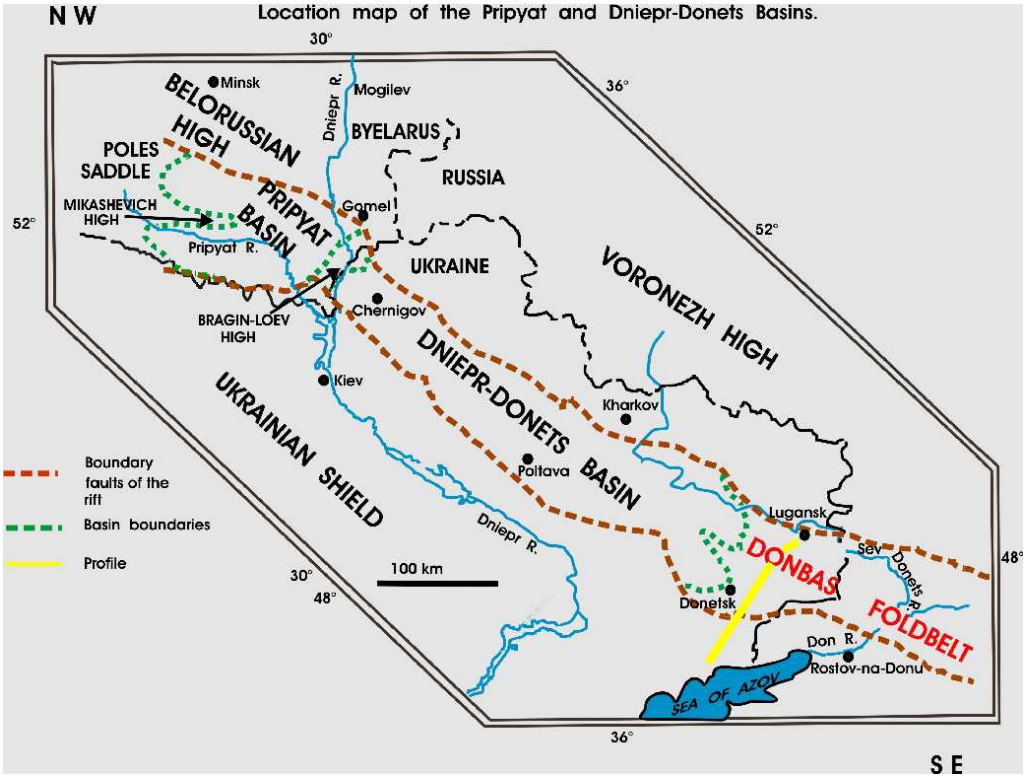

Figure 1: Location map of the survey area with major tectonic zones of the Dniepr-Donets basin. The yellow line shows the location of the profile.

The line was acquired in the framework of the DOBREflection 2000 project with the parameters illustrated in Table 1. The acquisition started in June and ended in September 2000. Detailed QC on the field was monitored by the University of Hamburg. Important considerations in the acquisition program included high fold, long receiver array lengths, and an offset range that corresponds to an angle of incidence from 0 to 45 according to the deepest target event. The area of the survey was 140 km and a total number of 877 shots were acquired with uniform shot spacing of 140 m interval. Along the profile the shooting interval was not always constant: in some areas there were shot point gaps, due to prohibition of shooting operations within an extensive network of coal mining. Each shot gather was made up of 680 traces with a geophone spacing of 35 m. In order to increase the signal-to-noise ratio and to suppress coherent surface waves the following standard processing steps were applied: trace editing and noise analysis, spherical divergence correction, surface consistent deconvolution, spectral balancing and residual static corrections.

RECORDING DATA

Record length	30 s
Sampling interval	2 ms
Channels	681
Geophone/Group	12
Gephone–Frequency	10 Hz

SPREAD

Type	split spread
Number of stations	681
Station interval	35 m
Minimum offset	35 m
Maximum offset	12000 m

VIBROSEIS PATTERN

Number of vibrators	4
Sweep frequency	8–80 Hz
Sweep length	12 s
Sweep type	linear
S.P. position	on half station
S.P. interval	140 m
Coverage	85 fold
Number of vert. stack/V.P.	20
Recording length	30 s

SPREAD DIAGRAM

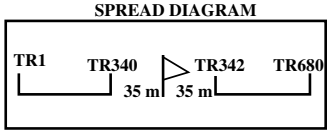

DYNAMITE PATTERN

Total charge size	80 kg TNT
Average hole depth	30 m
S.P. interval	variable
Coverage	4 fold
Recording length	99 s

Table 1: Seismic data acquisition parameters. The symbol S.P stands for shot point.

The data had a maximum frequency of 60 Hz with a central frequency close to 30 Hz. Special attention was given to preserving the large frequency bandwidth at all stages of processing. Figure 2 shows the first 3 s of two selected shot gathers before processing and Figure 3 shows the same shot gathers after processing. In Figure 3, the surface waves, high frequency signals at zero-offset and first arrival refractions are all suppressed. This figure demonstrates that the objective of enhancing the genuine reflection signals by suppressing coherent and random noise was well achieved. After processing the shot gathers were sorted to CMP gathers and were input into conventional stacking and CRS stacking.

SOME ASPECTS OF THE CRS METHOD

The CRS stack method uses a stacking operator that describes the reflection moveout response for inhomogeneous media. In contrast to CMP stacking, the CRS method does not depend on the stacking velocity model. The stacking curve is based on ray theory and for 2D it is given as (Mann et al., 1999):

$$t^2\left(x_m, P\right) = \left(t_0 + \frac{2\sin\alpha}{v_0}\left(x_m - x_0\right)\right)^2 + \\ + \frac{2t_0\cos^2\alpha}{v_0}\left(\frac{\left(x_m - x_0\right)^2}{R_N} + \frac{h^2}{R_{NIP}}\right), \quad (1)$$

where t_0 is the prestack zero-offset traveltime, x_0 is the location of the zero-offset ray on the surface, α is the angle of emergence of the normal incidence ray, R_{NIP} and R_N are the radii of curvature of two hypothetical wavefronts (Hubral, 1983), h is the half-offset between source and receiver, and x_m is the midpoint coordinate. P abbreviates the dependence of t on h, α, R_{NIP} and R_N. Equation (1) is equivalent to the conventional CMP stacking operator if x_m=x_0. For each sample (t_0, x_0) in the CRS section to be generated, the stacking parameter triplet $(\alpha,\, R_{NIP},\, R_N)$ that gives the optimal stacking operator is determined. These parameters are automatically searched through coherency analysis (Birgin et al., 1999). At first a preliminary zero-offset section is generated (automatic CMP stack). This section is used to determine the parameter triplet (i.e. wavefront attributes). The quality of the automatic CMP stack determines the quality of the estimated parameter triplets. With the optimum parameter triplet, the prestack data are stacked according to Equation (1) to give the CRS stacked section.

From experience the CRS stack results frequently require readjustment and fine tuning of some input control parameters like the range of possible α. The only required model parameter is the near

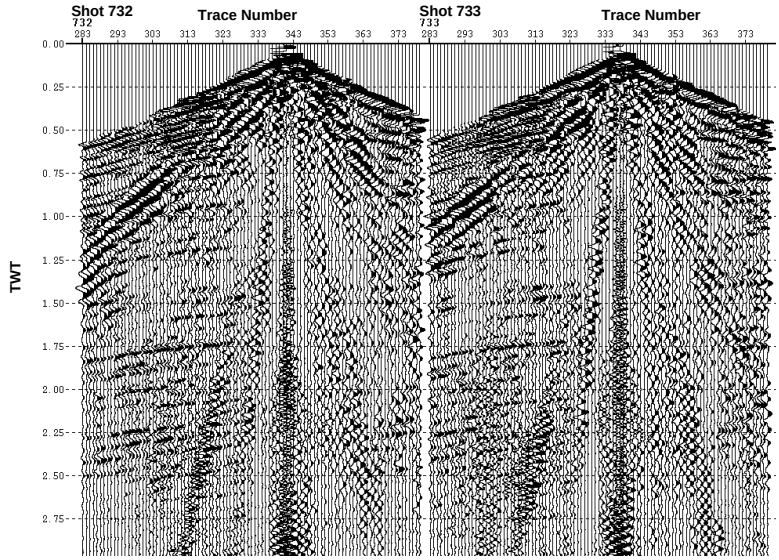

Figure 2: Two example shot gathers along the profile before processing. An automatic gain control (AGC) of 1000 ms was applied for display purposes. For shot 732 the source is located between channel 340 and 341 and for shot 733 the source is located between channel 339 and 340.

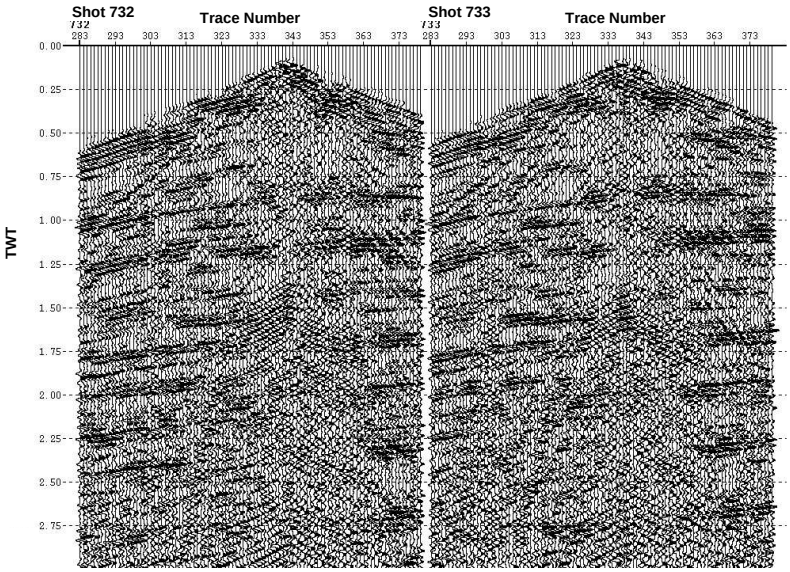

Figure 3: Same as in Figure 2 after processing. Almost all of the coherent noise are suppressed and genuine reflection events are enhanced.

surface velocity v_0. For the survey area this velocity was estimated from field statics and it was assumed to be constant along the line. Note that the image quality of the result does not depend on this average near surface velocity. We observed that using the constrained CRS strategy as described by Mann et al., (1999) reduces the run time and allows for a better estimate of the wavefront attributes. Apart from the stacked section, other by-products of the method are the coherency section, and wavefront attribute sections. The latter sections can be used for new inversion methods (Biloti et al., 2001). The former is used to interpret the consistency of the stacked result.

RESULTS

The CRS stack sections were migrated using the poststack Kirchhoff algorithm. The stacking velocities used for the common midpoint (CMP) stacking were converted to root mean square (rms) velocities. The rms-velocities were modified via rms-velocity analysis to give the optimum poststack time migrated section. The CRS stack and the CMP stack sections were migrated with the same rms-velocities. Poststack time migrated results of two zones are shown in Figures 4 and 5. Because the basin in-fill was inverted in the Permian age followed by erosion of younger sediments most of the sedimentary succession that outcrop right to the surface are of Carboniferous age. Figure 4a is the time migrated result after CMP stack and Figure 4b is the result after CRS stack. Note that, generally the imaging potential of poststack migration is limited by the quality of the stacked section. Therefore, improving the unmigrated stacked data quality via CRS stacking directly led to improved migration quality.

In Figure 4a only the main thrusted reflector is clearly imaged and the reflector continuity is disrupted. The marginal fault with back thrust is clearer imaged in Figure 4b than in Figure 4a. Steep dipping events (approximately 40^o) not clearly resolved in Figure 4a are enhanced. The change of reflector orientation near the surface indicates the out crop of the fault line. The surface location of this fault line was also seen in the structural geological section of the area. Also improved in the migrated section is the continuity of the main reflector between two way time 1.5 - 2.2 s. Note the enhancement of the near surface structure between TWT 0 - 0.7 s and trace numbers 0 - 210.

Figure 5a, b show the result of the main anticline in the northern part of the line. It is difficult to interpret the top and flanks of the anticline using Figure 5a. In Figure 5b the top of the anticline and other reflectors are better imaged. The improved quality of the CRS poststack migrated section is due to the improved quality of the CRS stack section. The improved quality and reflector continuity of the CRS stack section is caused by the increased fold of the CRS stacking operator. The layer boundaries in the migrated CRS images can be interpreted and used in an initial stage of prestack depth migration velocity analysis and subsequent model building techniques.

CONCLUSIONS

Our conclusion from this study is that in complex geology where CMP stacking and the subsequent poststack time migration fails, the CRS stacking and poststack time migration is a better alternative. Due to a better fit of the CRS stacking operator to the reflection events in the data, improved reflector continuities are achieved. The increased fold which is a result of the CRS stacking operator leads to an increase of the signal to noise ratio for shallow and deep reflectors. The information gained from the migrated CRS stacked section can be interpreted and incorporated in a velocity/depth model building flow.

ACKNOWLEDGEMENTS

This work was partly supported by the German Research Foundation (DFG, GA 350/9-1), and the sponsors of the *Wave Inversion Technology (WIT) Consortium*, Karlsruhe, Germany. We kindly thank Dr. Jürgen Mann (University of Karlsruhe) for providing the CRS stack code. Continuous discussions with the members of the Applied Geophysics Group Hamburg are highly appreciated.

Software used in this study include 2D Focus (seismic processing), Geodepth (prestack depth migration and velocity analysis) and the CRS code.

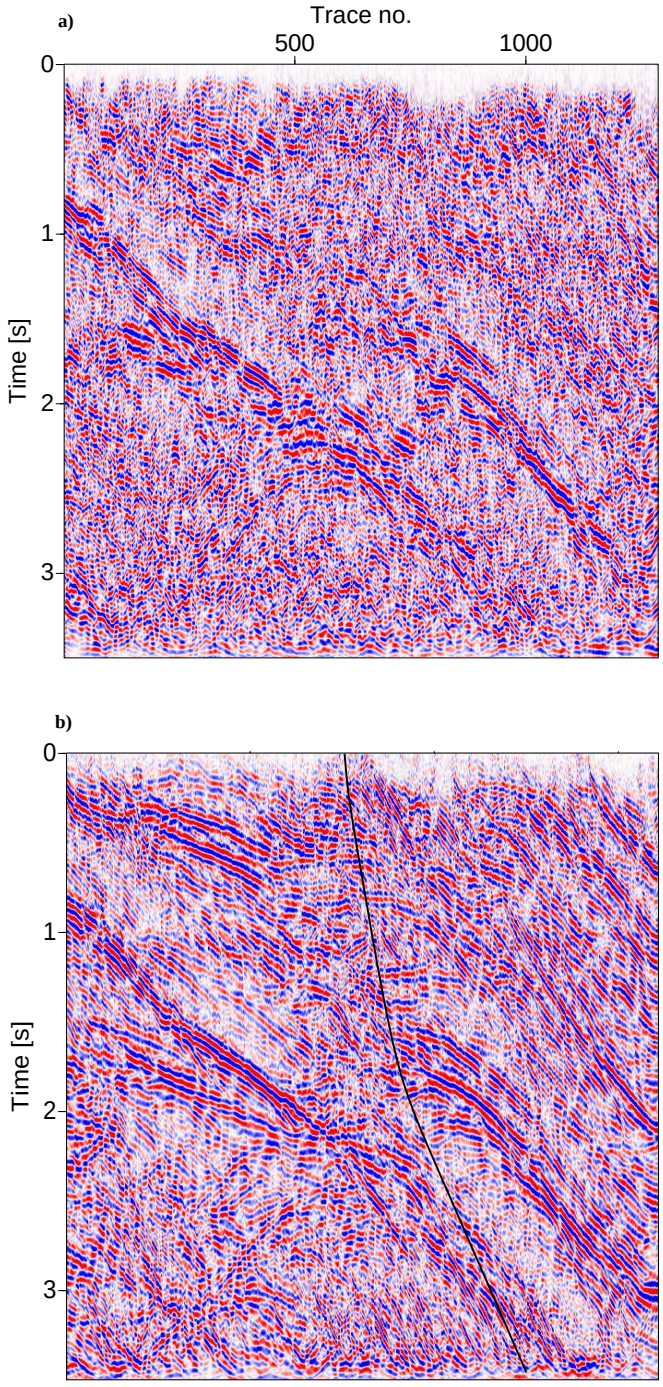

Figure 4: Poststack time migrated images of the main marginal fault zone after (a); conventional CMP stack and (b); after CRS stack.

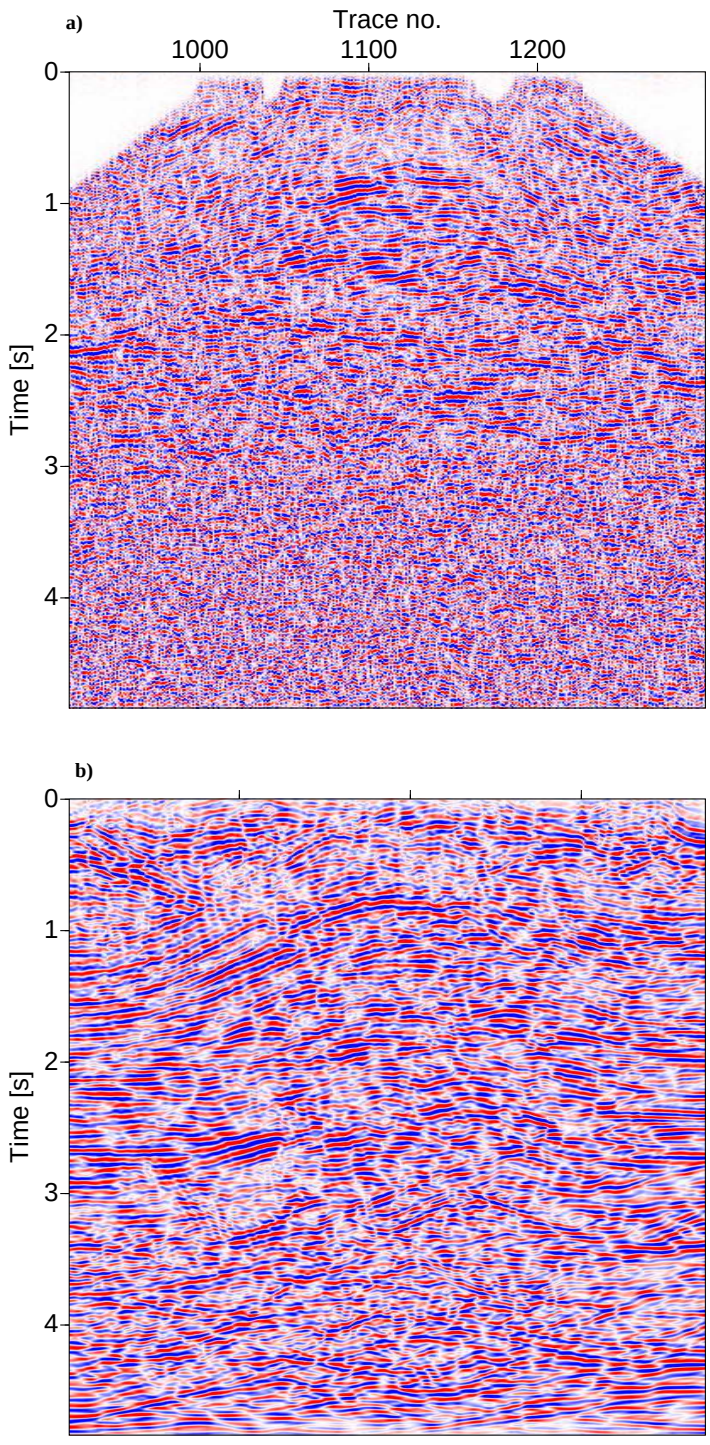

Figure 5: Poststack time migrated images of the main anticline after (a); conventional CMP stack and (b); after CRS stack.

REFERENCES

Biloti, R., Santos, L. T., and Tygel, M. (2001). Multiparametric traveltime inversion. *Wave Inversion Technology, Annual Report*, 5:51–63.

Birgin, E. G., Biloti, R., Tygel, M., and Santos, L. (1999). Restricted optimization: a clue to a fast and accurate implementation of the common reflection surface stack method. *Journal of Applied Geophysics*, 42(3,4):143–155.

Hubral, P. (1983). Computing true amplitude reflections in a laterally inhomogeneous earth. *Geophysics*, 48:1051–1062.

Mann, J., Hoecht, G., Jaeger, R., and Hubral, P. (1999). Common reflection surface stack - a real data example. *Journal of Applied Geophysics*, 42(3,4):301–318.

Stovba, S. M. and Stephenson, R. A. (1999). The Donbas Foldbelt: its relationship with the uninverted Donets segment of the Dniepr-Donets Basin, Ukraine. *Tectonophysics*, 313:59–83.